Supplemental Material: Robust Control of a Multifrequency Metamaterial Cloak Featuring Intrinsic Harmonic Selection

Yongjune Kim[1,2], Tianwei Deng[1,3], Wei Xiang Jiang[4], Tie Jun Cui[4], Yongshik Lee[5,*], and Cheng-Wei Qiu[1,†]

[1] *Department of Electrical and Computer Engineering, National University of Singapore, Singapore 117583, Singapore*
[2] *Center for Advanced Meta-Materials, 156 Gajeongbuk-ro, Yuseong-gu, Daejeon 34103, South Korea*
[3] *Temasek Laboratories, National University of Singapore, Singapore 117411, Singapore*
[4] *State Key Laboratory of Millimeter Waves, Southeast University, Nanjing 210096, P. R. China*
[5] *Department of Electrical and Electronic Engineering, Yonsei University, Seoul 03722, South Korea*

1 Optimization procedure of scaling factors

The column and row scaling factors multiplied to refractive indices of the cloak are determined via a flow chart in Fig. S1. Based on the function of parametric sweep in the commercial finite element method (FEM) solver COMSOL Multiphysics, the optimal scaling factors β_j and γ_i are determined by minimizing the normalized scattering width (SW).

Finally, the refractive indices included in each sector are scaled by $\zeta_{i,j}$ to correct the variation of α in the same row and column. The final scaling factors β_j, γ_i, and $\zeta_{i,j}$ are summarized in Table 1, 2, and 3, respectively.

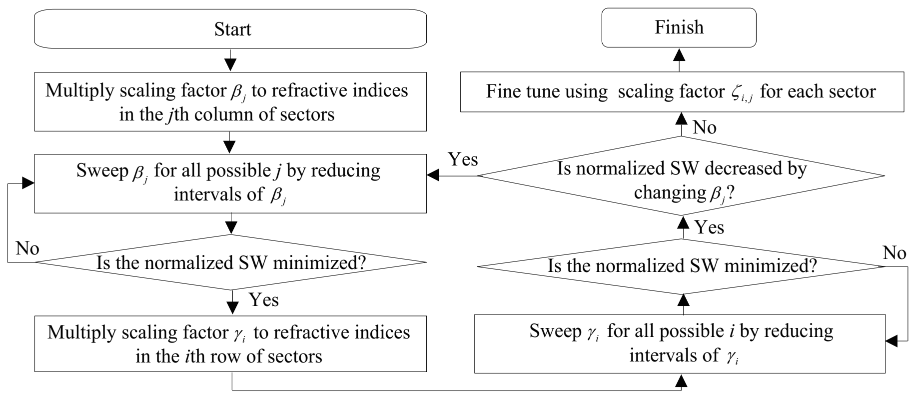

Figure S1: A flow chart to determine optimal scaling factors.

Table S1: Optimized scaling factors β_j from $j = 1$ to $j = 6$.

	$j = 1$	$j = 2$	$j = 3$	$j = 4$	$j = 5$	$j = 6$
β_j	0.72	0.77	0.84	0.95	1.05	1.05

Table S2: Optimized scaling factors γ_i from $i = 1$ to $i = 5$.

	$i = 1$	$i = 2$	$i = 3$	$i = 4$	$i = 5$
γ_i	1	0.98	1.04	1.03	1.01

Table S3: Optimized scaling factors $\zeta_{i,j}$ from $j = 1$ to $j = 6$ as well as from $i = 1$ to $i = 5$.

$\zeta_{i,j}$	$j = 1$	$j = 2$	$j = 3$	$j = 4$	$j = 5$	$j = 6$
$i = 1$	0.99	1	0.99	1.01	1	1
$i = 2$	1.01	1	1	0.99	1	1.01
$i = 3$	·	·	1.01	1	0.99	0.99
$i = 4$	·	·	·	0.99	1.01	1.01
$i = 5$	·	·	·	·	1	0.99

2 Simulation results of cloaks for various heights of diamond objects

Figs. S2(a) and (b) show the optimized refractive index profiles of the cloaks for the diamond objects of which the heights are 80 and 120 mm, respectively. The heights of the cloaks h_{cloak} are determined to 116 mm for h_{obj}=80 mm and 156 mm for h_{obj}=120 mm. As the cloak in Fig. 1(d) in the paper, the upper and bottom boundaries of the cloaks are set to include three arrays of $6{\times}6$ mm^2

*yongshik.lee@yonsei.ac.kr
†chengwei.qiu@nus.edu.sg

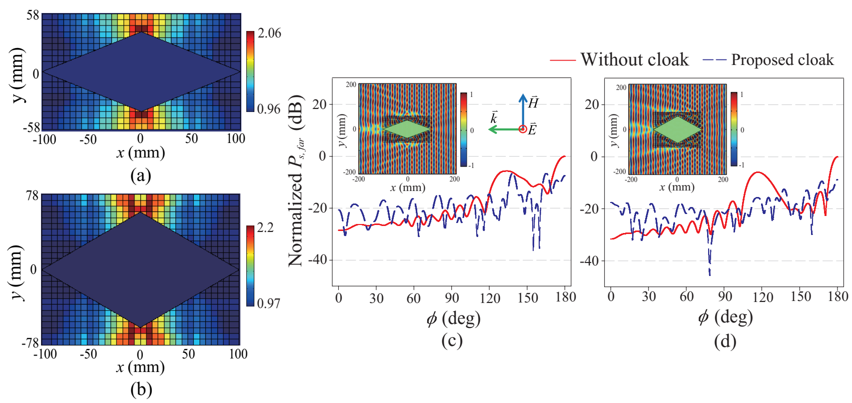

Figure S2: Optimized refractive index profiles for (a) h_{obj}=80 mm and (b) h_{obj}=120 mm. Normalized far-field scattering patterns for (c) h_{obj}=80 mm and (d) h_{obj}=120 mm with and without cloaks of Figs. S2(a) and (b), respectively. Insets: Full-wave simulation results with proposed cloaks.

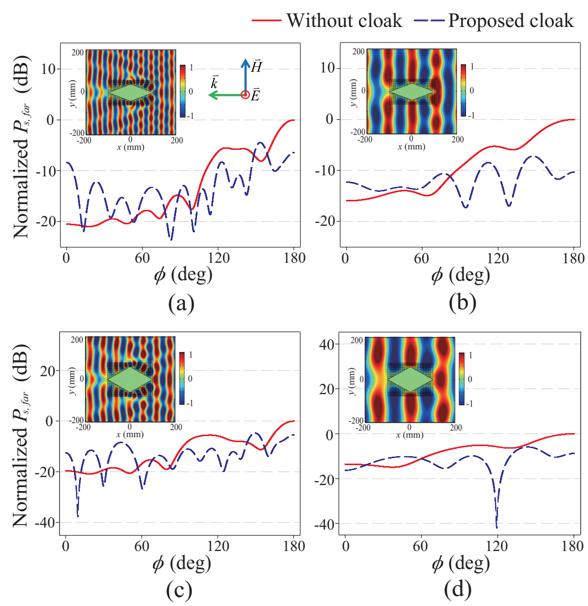

Figure S3: Normalized far-field scattering patterns with and without cloaks at (a) 6.6 GHz and (b) 2.8 GHz for h_{obj}=80 mm and at (c) 5.1 GHz and (d) 2.1 GHz for h_{obj}=120 mm.

pixels from the top and bottom vertices of the diamond objects. The number of arrays guarantees the function of controlling the path of the wave inside the cloak without extremely large refractive index. The refractive indices slightly

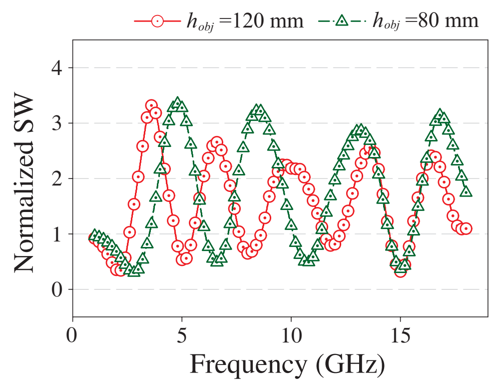

Figure S4: Normalized scattering widths vs frequency for h_{obj}=80 and 120 mm.

less than one in Figs. S2(a) and (b) can be removed by adding a condition in the optimization process that the scaling factors $\beta_{j=6}$ and $\zeta_{i,j=6}$ do not decrease less than one.

Figs. S2(c) and (d) show the far-field scattering patterns of the diamond perfect conductor (PEC) of which the heights are 80 and 120 mm, respectively, with and without the cloaks. The patterns in Figs. S2(c) and (d) are normalized by the peak level of each diamond PEC. The insets are the full-wave simulation results of both of the proposed cloaks at the design frequency 15 GHz. Although the backward scatterings are increased with the cloaks due to the impedance mismatch in low levels, the forward scatterings are reduced excellently by the cloaks. The normalized SWs of the cloaks are calculated as 0.365 for Fig. S2(c) and 0.319 for Fig. S2(d).

Figs. S3(a) and (b) show the normalized far-field scattering patterns for the diamond PEC of h_{obj}=80 mm with and without the cloak at 6.6 and 2.8 GHz, respectively, where the normalized SWs are minimized. The normalized SWs are 0.485 at 6.6 GHz and 0.296 at 2.8 GHz. Likewise, Figs. S3(c) and (d) show the results for h_{obj}=120 mm at 5.1 and 2.1 GHz where the normalized SWs are minimized as 0.551 and 0.321, respectively.

Fig. S4 shows the calculated normalized SWs of the proposed cloak vs frequency for h_{obj}=80 and 120 mm. The results show that the cloaking harmonics can be tuned in almost whole frequency range below the design frequency 15 GHz by changing the height of the diamond PEC. Besides, the normalized SW of 0.48 at 10.7 GHz for h_{obj}=80 mm indicates that the scattering reductions at the cloaking harmonics can be improved by reducing the height of the hidden object. This is because the internal reflections at the boundaries of the pixels inside the cloak are mitigated by reducing the variation of refractive index. For example, the highest refractive index inside the cloak is decreased from 2.3 to 2.06 by reducing the height of the diamond object. On the other hand, the normalized SWs calculated as 0.736 and 0.847 at 12 and 7.9 GHz for h_{obj}=120 mm indicate that there remain relatively high scatterings. This is because the high variation of the refractive index causes non-negligible internal reflections similar with the case of h_{obj}=100 mm in the paper.

3 Simulation results of metamaterial unit cells

To match the refractive indices in Fig. 1(d) in the paper to the radially symmetric 3D structure, the refractive index matched to the radius of the drilled hole structure in Fig. S5(a) are used. Fig. S5(a) indicates the effective refractive indices of the drilled-hole structures vs radius for various thicknesses of FR4 substrates. Fig. S5(b) shows the imaginary parts of the refractive indices. Fig. S5(b) is used to simulate the two-dimensional (2D) lossy cloak of Figs. 4(a)-(c) in the paper. The right-hand side of Fig. S5(b) is a subwavelength cuboid unit cell of the drilled-hole structure. The height of it along the z axis is 6 mm while the widths along both of the x and y axes are 3 mm. The empty spaces at the top and bottom sides of the substrate are filled with air.

Fig. S6 shows additional simulation results of a fan-shaped metamaterial unit cell proposed in the paper. The curves indicate the refractive indices vs

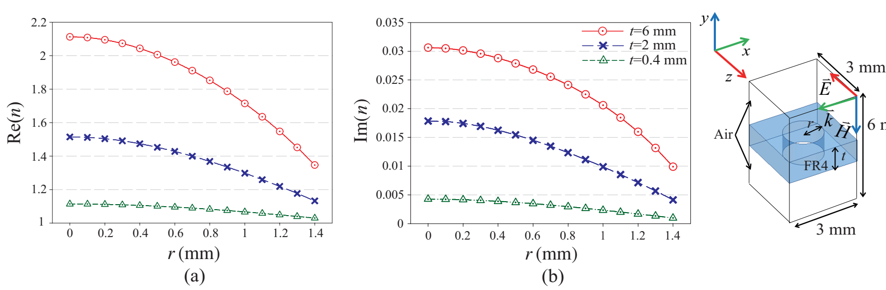

Figure S5: Effective refractive index of drilled-hole structure vs radius of it for various thickness of FR4 substrate. (a) Real and (b) Imaginary parts. Right-side panel: A cuboid unit cell.

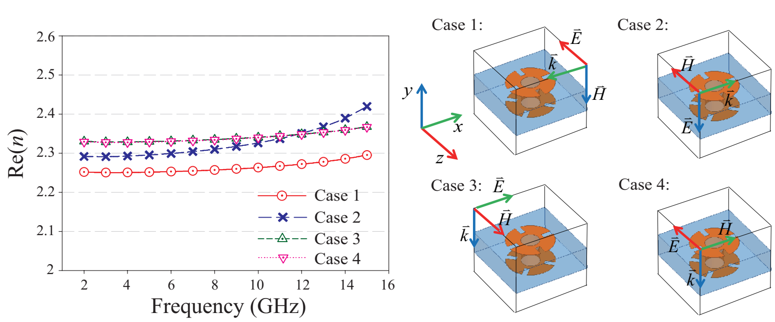

Figure S6: Refractive indices of fan-shaped metamaterial unit cell for various polarizations.

frequency for all of the possible orthogonal polarizations of incident electromagnetic (EM) waves. The right-hand side of Fig. S6 shows all of the cases. The case 1 in the panel is the same with Fig. 3(b) in the paper. The polarization of case 2 is orthogonal with that of the case 1 while the direction of the propagation is parallel with each other. The refractive index of the case 2 at 15 GHz is 2.42 which is 5.7% larger than 2.29 of the case 1. The wave vector of the case 3 is orthogonal with that of the case 1, and the polarization of the case 4 is orthogonal with that of the case 3. Both of the refractive indices for the cases 3 and 4 are identically confirmed as 2.367 due to the symmetric configuration of the structure, which is 3.4% larger than that of the case 1. The remained two cases of which the wave vectors are along the y axis are omitted here because the responses of them are identical with those of the cases 1 and 2. Although different responses are confirmed among the cases, the differences are negligible. Therefore, almost identical refractive indices independent of the polarizations are verified.

4 Fabrication of 3D cloak

Fig. S7(a) shows the first layer from the upper or bottom boundaries of the cloak. It consists of FR4 substrates which have different thicknesses t of 0.4, 2, and 6 mm as indicated in Fig. S7(a). The substrate of t=6 mm is fabricated

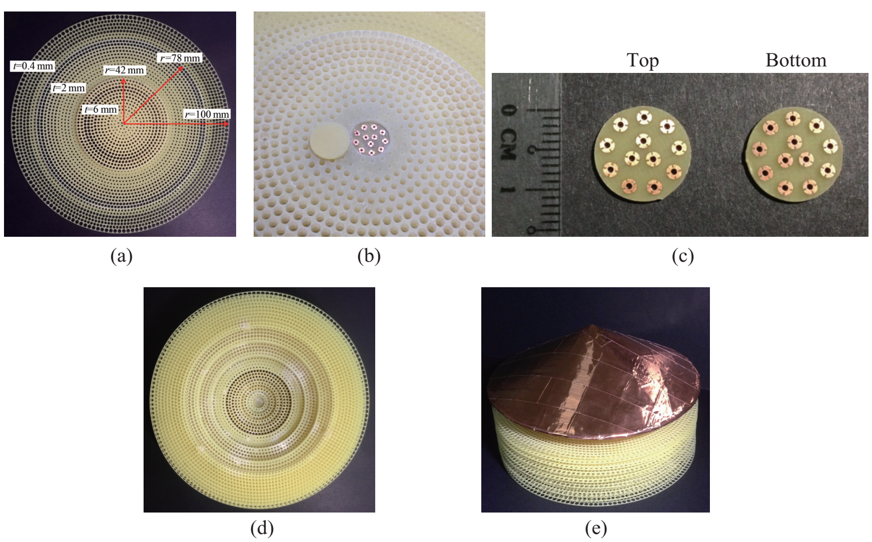

Figure S7: Fabricated cloak with FR4 substrates. (a) A layer consists of FR4 substrates in which cylindrical hole arrays are drilled. (b) A view of a layer including fan-shaped metamaterial. (c) Top and bottom views of fan-shaped copper patches. (d) A view of the interior region of fabricated cloak. (e) A copper double cone combined with fabricated cloak.

by stacking the substrate of t=2 mm. For the refractive indices of the pixels adjacent to $x = \pm 100$ mm of Fig. 1(d) in the paper, the radius of the hole is determined by using a unit cell that has 4×4 mm^2 area rather than that of Fig. S5 which has 3×3 mm^2 area. Because a hole array near the outer edge of the substrate of t=1 mm is almost adjacent to the boundary of the substrate, the cylindrical hole is transformed to curved rectangular one by maintaining the volume of the hole.

Fig. S7(b) shows the part of the layer that includes the refractive index larger than that of FR4. The layer is composed with holes as well as fan-shaped metamaterial. Fig. S7(c) shows the half of the fabricated cloak that is assembled with drilled-hole layers. The layers are connected by small FR4 pillars. The conical region of the copper double cone is adjacent to the center of the FR4 disk, in which the fan-shaped metamaterial is involved. Fig. S7(d) shows the copper double cone combined with the fabricated cloak.

5 A measurement system

Fig. S8 shows a measurement system consisting of two broadband horn antennas as well as two lenses in anechoic chamber, which can measure the EM wave from 2 to 18 GHz. The scattering (S) parameter, S21, was measured by a PNA N5244A of Agilent technologies. By using the lens, the EM waves can be focused with the plane wavefront at the location of the sample. To measure the far-field scattering, both of the lenses are separated by 1.07 m from the sample. The antennas are set to transmit and receive the vertical polarization. To match the measurement condition with that of simulation, the fabricated structure is put on the sample holder as shown in Fig. S8. The sample holder is composed with polystyrene foams. Based on the measurement setting in Fig.

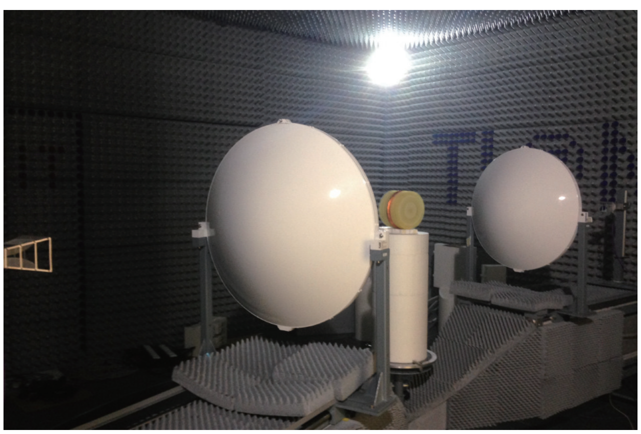

Figure S8: A system for measurements of far-field scattering patterns inside an anechoic chamber.

S8, a relative scattered power can be measured in the azimuthal plane via the scattering (S) parameter, S21. By subtracting S21 measured in the free space condition from that measured with an object, a relative far-field scattered power can be measured.